CIRP Annals - Manufacturing Technology 00 (2020) 1–4

Contents lists available at ScienceDirect

CIRP Annals - Manufacturing Technology

journal homepage: https://www.editorialmanager.com/CIRP/default.aspx

Oxide dispersion strengthened 304 L stainless steel produced by ink jetting and laser powder bed fusion

Brian K. Paul[a,c,*], Kijoon Lee[a,c], Yujuan He[b], Milad Ghayoor[a,c], Chih-hung Chang[b], Somayeh Pasebani[a,c]

[a] School of Mechanical, Industrial and Manufacturing Engineering, Oregon State University, Corvallis, OR, 97330, US
[b] School of Chemical, Biological and Environmental Engineering, Oregon State University, Corvallis, OR, 97330, US
[c] Advanced Technology and Manufacturing Institute (ATAMI), Oregon State University, Corvallis, OR 97330, US

Submitted by Neil Duffie (1), Madison, U.S.

ARTICLE INFO

Article history:
Available online xxx

Keywords:
Additive manufacturing
Metal matrix composite
Stainless steel

ABSTRACT

This paper discusses the fundamentals of a novel hybrid method to synthesize oxide dispersion strengthened (ODS) 304 L stainless steel (SS) alloy using a modified laser powder bed fusion (LPBF) machine. Previously, ODS metal matrix composites have been produced by LPBF via ball-milling, which is expensive to scale. Here, we selectively dope yttria nanoparticles into a SS matrix by jetting a precursor chemistry onto the SS substrate prior to laser conversion and consolidation. The new alloy shows good room temperature mechanical properties. Microstructures are studied using electron microscopy, energy dispersive spectroscopy and electron backscatter diffraction.

1. Introduction

Additive manufacturing (AM) processes are used to build mechanical components by depositing materials layer-by-layer [1]. Among metal AM processes, powder bed fusion (PBF) has the most widespread set of applications [2]. PBF methods use either a laser or electron beam to fuse a metal powder layer at the top of a powder bed to the layer below. A well-known application for laser PBF (LPBF) is the fuel nozzle within the leading edge aviation propulsion engine advanced by General Electric in which a conventional design of about 20 parts was reduced to a single LPBF build [3]. While these advancements are significant, the current LPBF build practice in industry is generally limited to single alloys. In contrast, directed energy deposition processes have been used to fabricate metal composites that can be used for producing highly engineered mechanical components requiring more than one material [4].

ODS alloys are metal-matrix composites in which nano-scale oxides inhibit grain growth at high temperatures providing high temperature mechanical properties and high creep resistance [5]. ODS ferritic alloys are of interest to the nuclear industry as an alternative to radiation-tolerant cladding and structural materials. The small size and high number density of oxides leads to a large number of composite interfaces, which are thought to annihilate point defects, preventing the clustering of defects prior to failure [6]. However, ODS alloys are challenging to cast due to buoyancy of the particles [7]. As a result, traditional powder metallurgy is used for producing ODS alloys, which necessitate tens of hours of ball-milling to produce modest volumes of material [8]. Furthermore, post-sintered welding of ODS alloys poses similar challenges to those in casting [8].

LPBF has been used to produce ODS alloys [7,9], using the faster solidification rates and high surface tension gradients to overcome buoyancy and agglomeration issues. However, these studies used ball-milling to distribute oxides within the powder bed resulting in monolithic components that cannot be welded.

This paper investigates the process fundamentals for a hybrid LPBF process that uses inkjet technology and laser consolidation to dope an oxide phase into the metal matrix as it is being built. This selective doping of the material enables two advantages. First, it eliminates the need to ball mill the powder making the process more scalable. Second, it enables the "turning on/off" (i.e. "programming") of mechanical properties during LPBF builds, e.g. allowing nuclear engineers to specify oxide-free regions requiring welding but no radiation-resistance. In so doing, the process opens the potential to vary material properties throughout monolithic structures. The following sections describe the investigation of using ink jetting with, first, laser cladding, and then LPBF, to produce a 304 L SS ODS alloy.

2. Materials and methods

2.1. Laser cladding

ODS 304 L SS was chosen due to its excellent thermal stability and high temperature mechanical properties [10]. Preliminary experiments to evaluate ink development were conducted using a Sandvik

* Corresponding author.
E-mail address: brian.paul@oregonstate.edu (B.K. Paul).

https://doi.org/10.1016/j.cirp.2020.04.071
0007-8506/

Osprey gas-atomized AISI 304 L austenitic SS powder, characterized using dynamic light scattering (powder size: 15–45 μm). A laser cladding setup, involving the use of a 1000 W Rofin FL010 laser welder (1080 nm), was used to accelerate sample preparation and characterization. Dopant ink, consisting of yttrium oxide nanoparticles (NPs) suspended in a solvent, was jetted into a single layer of powder (50 μm thick), which was laser clad to an underlying 304 L SS substrate. The powder layer was placed onto the substrate manually using a doctor knife and template. To simulate an LPBF environment, the substrate was placed within a vacuum canister used to keep oxygen levels <100 ppm to avoid an enlarged melt pool size caused by exothermic oxidation of Fe [11]. The canister consisted of a vacuum flange sealed with an IR-transparent quartz plate and permitted the flow of ultra-high purity argon (99.999%) to purge the cladding atmosphere after sample placement. An oxygen sensor (Rapidox 1100Z) was used to monitor oxygen levels before and during cladding.

The first experiment investigated the effect of the placement of NPs within the powder bed on material microstructure. The NP ink was prepared ex-situ by suspending one wt% of yttrium oxide (Y_2O_3) NPs (procured from US Research Nanomaterials, Inc.) in a mixture of ethanol (C_2H_6O) and ethylene glycol ($C_2H_6O_2$). In the first set of experiments, the ink was jetted into the powder bed using an artist's airbrush. In the second set of experiments, the ink was jetted onto the substrate and allowed to dry prior to layering the powder. After

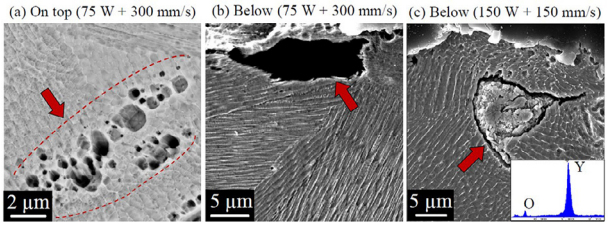

Fig. 1. SEM micrographs showing various defects indicated by arrows within the cross-section of sample produced by placing the ex-situ ink on (a) top and (b, c) below the powder layer.

layering, the powder bed was laser clad to a SS substrate. Laser powers of 75 and 150 W and scan speeds of 150 and 300 mm/s were utilized. A subset of scanning electron microscope (SEM) images are shown in Fig. 1.

The spherical shape and size of the pores, in the samples in which NPs were placed on top of the powder bed, suggest pores were likely the result of evaporated solvent within the melt pool (Fig. 1a). Much larger pores were located mainly at the top of the cladding even when NPs were placed on the bottom (Fig. 1b). Energy dispersive X-ray spectroscopy (EDS) confirmed the source of these larger pores as large oxide agglomerates (Fig. 1c).

Two findings were drawn from this experiment. First, for the samples with NPs placed on top, the lack of agglomeration was explained by good dispersion of the ink into the powder bed due to wicking penetration. However, the solvent did not fully evaporate from the bed prior to cladding, due to high surface energy in the bed. Therefore, when the bed was laser irradiated, the remaining solvent flash evaporated leaving pores. Second, for the samples with the NPs jetted below the powder bed, the larger pores were likely caused by oxide agglomerates that fell out during metallography. The agglomerates likely formed during layering and floated to the top of the melt pool.

Subsequently, one additional experiment was performed to further investigate these hypotheses. First, to eliminate gas porosity, as before, the NP ink was jetted onto the substrate and allowed to dry by preheating the substrate in a hot oven at 100 °C for 10 h prior to layering of the powder. Second, to prevent NP agglomeration, efforts were made to anchor the NP ink onto the substrate by irradiating the NPs on the substrate with a volumetric energy density (VED) of 83 J/mm^3 (75 W; 300 mm/s) to sinter them to the substrate prior to powder layering.

Fig. 2a shows that this procedure eliminated the larger pores at the top of the laser cladding. However, a carbon-rich (83.5 at%) layer

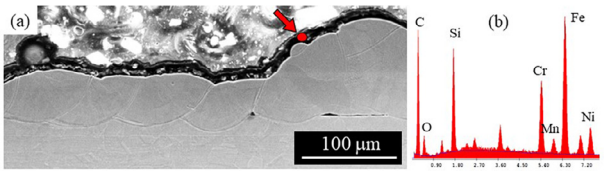

Fig. 2. (a) SEM image showing no observation of yttria agglomeration on top after changing the process step (power 75 W and speed 300 mm/s) and (b) EDS point analysis on the carbon layer (indicated by arrow).

was observed at the top of the fusion zone as identified by an EDS point analysis. This layer was attributed to a residue from the organic surfactants used to suspend the NPs. To eliminate the use of surfactants, a second precursor ink was developed to enable the synthesis of the NPs in-situ during laser cladding. Apart from eliminating the need for surfactants and carbon contamination, this method also reduced the likelihood of clogging the jetting mechanism. Further, the new ink used less solvent, reducing jetting and evaporation time prior to cladding.

The precursor ink consisted of yttrium nitrate hexahydrate $Y(NO_3)_3$ in methanol (CH_3OH) with a concentration of 1.83 mol/L. Methanol was used as a solvent (instead of ethanol) since methanol has a higher solubility with the precursor and reduces evaporation time due to a higher vapor pressure and lower boiling point. The thermal decomposition of the precursor ink is described in [12]. To validate the conversion of the ink, the precursor ink was baked in a hot oven at 600 °C for an hour and analyzed by X-ray diffraction (XRD), which shows the yttria peak at 29° (Fig. 3a). Next, to confirm laser conversion of the precursors, the precursor ink was deposited on a SS 304 substrate and irradiated at a VED of 333 J/mm^3 (150 W;

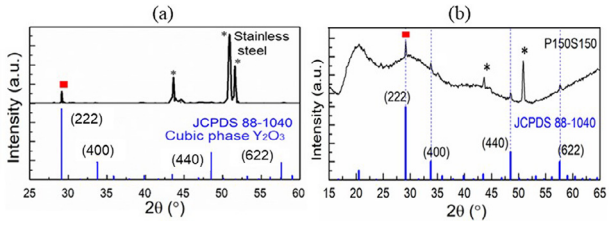

Fig. 3. XRD results: (a) heating at 600 °C for one hour, (b) laser cladding.

150 mm/s). Next, the SS 304 powder was layered, followed by laser cladding (333 J/mm^3; 150 W; 150 mm/s) for melting and mixing. Fig. 3(b) confirms yttria conversion from the application of laser energy.

Fig. 4(a) shows the SEM cross-sectional microstructure of the ODS 304 L SS alloy fabricated by hybrid laser cladding, after electropolishing and etching. The yttria particles are in a size range between 20–100 nm. As shown in the scanning transmission electron micrograph (STEM) of Fig. 4b, the particles were identified as a compound of Y-Si-O having better thermal stability than Y_2O_3 [8]. These compounds are similar to NPs observed from [13,14] that produced ODS 304 L alloy via ball-milling followed by LPBF. Vickers microhardness (HV) was evaluated on the cross-sections of the fusion zone with a

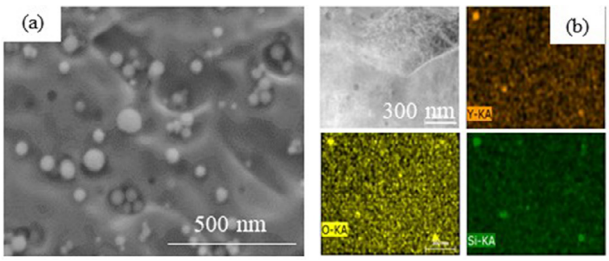

Fig. 4. (a) Precipitation of spherical nanoparticles from hybrid laser-clad 304 SS + 4 wt.% yttria and (b) STEM-EDS elemental map of hybrid laser clad ODS 304 L showing Y, O and Si.

Please cite this article as: B.K. Paul et al., Oxide dispersion strengthened 304 L stainless steel produced by ink jetting and laser powder bed fusion, CIRP Annals - Manufacturing Technology (2020), https://doi.org/10.1016/j.cirp.2020.04.071

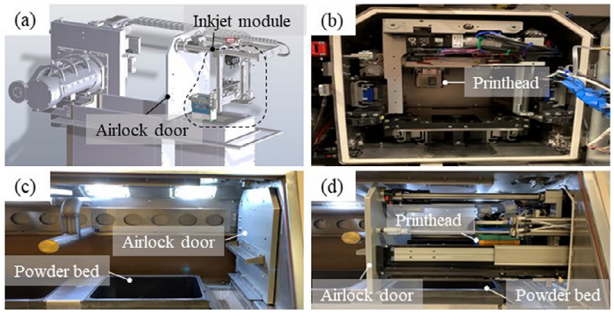

Fig. 5. (a) Solid model of hybrid system, (b) end view of airlock showing installed Xerox module, (c) before and (d) after Xerox module extending over powder bed chamber.

load of 50 gf and a dwell time of 15 s. Microhardness was found to be 188 ± 4, 210 ± 7 and 256 ± 15 HV, for the annealed, laser-clad 304 SS and laser-clad ODS samples, respectively, an increase of 12% and 36%, respectively.

2.2. LPBF tool modifications

Tensile test bars were produced using a commercially-available LPBF tool (3D Systems ProX DMP 300) modified to enable inkjetting of the precursor ink into the powder bed prior to laser consolidation. The modification involved integrating a single-ink piezoelectric inkjet unit (Xerox M Series, 880 nozzles, 300 dpi) into the LPBF tool. The inkjet module was installed within the airlock (Fig. 5a, b) used to load and unload the build plate without disturbing the inert environment in the build chamber. Fig. 5c,d show the airlock door position during layering/consolidation versus jetting, respectively.

Furthermore, the ProX 300 control software was modified to operate synchronously with the inkjet mechanism enabling the sequencing and parameterizing of the layering, jetting and consolidation steps. Xerox control software was used off-line to set jetting parameters (e.g. ink reservoir temperature, firing frequency, number of active nozzles, etc.) and was modified to coordinate print head positioning with the firing of jets. A third controller, setup on an external laptop, was linked to the servo controller for managing the speed and position of the printhead. Once the servo controller received a signal from the ProX 300, the inkjet printhead moved into position at which point the servo controller sent a signal to the Xerox controller to begin jetting.

2.3. Specification of the ink

Next, efforts were made to calibrate jetting of the ink. First, an average droplet mass and volume were determined, as a function of jetting frequency (5–15 kHz), using catch-and-weigh and a high-speed video camera. Results show that the mass and volume of the droplets were the lowest at a frequency of 5 kHz. Tensile bars were built at 5 kHz to maximize the surface-to-volume ratio of the droplets and, thereby, accelerate solvent evaporation. Second, efforts were made to calculate droplet mass needed to achieve the desired wt% of yttria within the powder bed. Assuming a frequency of 5 kHz, 0.5 wt% yttria was calculated to require a print scan speed of 20 mm/s. An experiment was conducted using these conditions and the average ink mass from experimental measurements was found to be 5.4% higher than calculated. This uncertainty was considered acceptable for producing the material.

2.4. Tensile bar fabrication

Three blocks ($110 \times 11 \times 5\ mm^3$) of ODS alloy were built parallel to the surface of the build plate using the hybrid LPBF tool and the precursor ink. The process sequence involved jetting the precursor on the metal substrate followed by laser NP synthesis and mixing, powder layering and laser consolidation. No delay was required for solvent evaporation.

The process parameters used for both laser steps were 175 W, 1000 mm/s, 75 μm, and 40 μm for the power, scan speed, hatching space, and the layer thickness, respectively (VED = 58 J/mm^3). Two tensile test samples were produced from each block via wire electro-discharge machining. Following the ASTM E8 standard, all six samples had a thickness of 1.6 mm and a gage width and length of 6.0 and 32.4 mm, respectively. Additionally, three blocks of LPBF 304 L SS without oxide dispersants were fabricated using the same machine and parameters without the jetting step. The microhardness was measured on the cross-section of the fusion zone. An Instron 5969 universal tester was used to measure mechanical properties for five LPBF 304 L SS samples and five LPBF ODS 304 L samples. Relative densities were measured by Archimede's method.

3. Results and discussion

Fig. 6(a) shows the microstructure after electrochemical etching having well-distributed spherical precipitates of a similar size to the NPs found in Fig. 4. The micrographs show no evidence of gas porosity suggesting no issues with solvent evaporation. The relative densities of the LPBF 304 L and LPBF ODS 304 L samples were found to be 97.2% ± 0.4 and 97.8% ± 0.2, respectively (non-optimized). These

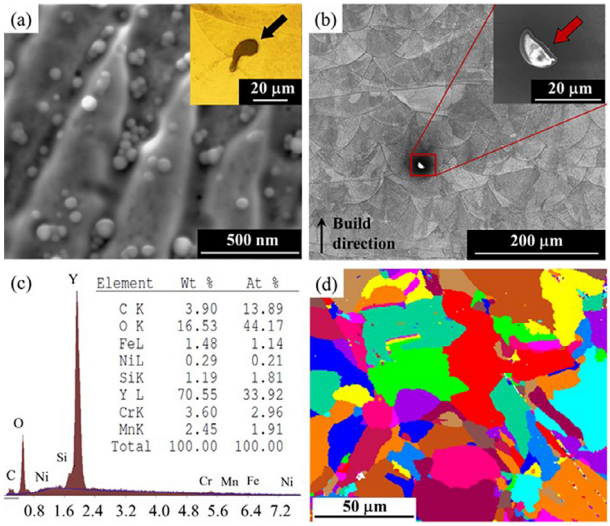

Fig. 6. (a) nano-scale precipitates with inset void, (b) cross-section perpendicular to scanning direction showing oxide scale (inset at higher magnification), (c) EDS spectrum (Y/Si/O), (d) EBSD grain map of cross-section perpendicular to build direction of ODS 304 L specimen.

densities further support that ink addition did not increase porosity. A few irregular-shaped pores were observed (Fig. 6a inset) similar in size and shape to the oxide voids caused during metallography. This is consistent with a few yttrium silicate inclusions [13] of similar size observed intermittently (Fig. 6b and inset and Fig. 6c).

The grain structure perpendicular to the build direction was studied by electron backscatter diffraction (Fig. 6d). The average grain sizes were 6.1 ± 4.8 μm and 5.8 ± 4.1 μm for LPBF and LPBF ODS samples, respectively. The smaller grain size may be due to oxides acting as inoculants, increasing heterogeneous nucleation sites [15]. The measurements do not show statistically significant grain refinement for the ODS 304 L alloy.

Microhardness measurements for the annealed, LPBF and ODS LPBF samples were 174 ± 4, 252 ± 8 and 272 ± 6 HV, which is a 45% and 56% increase, respectively. Tensile test results are shown in Fig. 7 and summarized in Table 1. Yield strength (YS) improvements for the LPBF 304 L SS and the LPBF ODS 304 L alloy were 231% and 245%, respectively, compared to wrought 304 L SS. The LPBF YS is 31% higher than previous work found at similar grain size and porosity [10] likely due to better wettability. The YS found is more on par with "nearly fully dense" LPBF 304 SS samples produced in [16], which did not report grain size nor density. The LPBF ODS YS is on par with prior

Please cite this article as: B.K. Paul et al., Oxide dispersion strengthened 304 L stainless steel produced by ink jetting and laser powder bed fusion, CIRP Annals - Manufacturing Technology (2020), https://doi.org/10.1016/j.cirp.2020.04.071

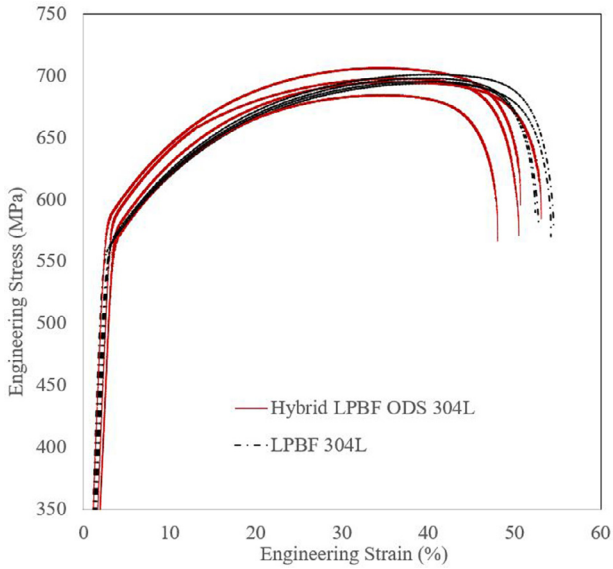

Fig. 7. Stress strain curves for LPBF ODS and LPBF 304 L specimen.

Table 1
Mechanical properties of LPBF ODS, LPBF and wrought 304 L SS.

Material	YS (MPa) (0.2% offset)	UTS (MPa)	El (%)
Hybrid LPBF ODS 304L	586 ± 9	695 ± 9	51 ± 3
LPBF 304L	562 ± 11	701 ± 4	54 ± 1
Wrought 304 L [18]	170	484	40

ODS 304 SS YS of similar density produced by powder metallurgy, hot isostatic pressing (HIP) and forging [17]. LPBF and LPBF ODS results show similar ultimate tensile strengths and elongations. The 51% elongation in the ODS sample is 108% greater than prior HIP work [17].

The increase in mechanical properties of both LPBF samples is likely due to microstructural refinement and high dislocation density associated with fast cooling rates. Given similarities in porosity and grain size of the LPBF and ODS LPBF samples, the increased YS at room temperature of the ODS sample is likely due to oxide precipitates further impairing dislocation motion. Further efforts are needed to optimize laser parameters for precursor conversion, precipitate sizing and reduced porosity. Finally, it is noted that ODS materials, while providing some enhancement in mechanical properties at room temperature, typically provide enhancement in mechanical properties at high temperatures. Therefore, additional work is needed to evaluate the mechanical and creep properties of these materials at high temperature.

4. Conclusions

A new method for fabricating an ODS 304 L SS alloy was demonstrated using a commercially-available LPBF machine tool modified with inkjet technology. Preliminary results show the need to move away from surfactant-dispersed inks toward the use of chemical precursors and in-situ synthesis of precipitates. Spherical Y-Si-O precipitates with good thermal stability were produced within a matrix of 304 L SS. Increased room temperature hardness and YS of the LPBF ODS alloy was attributed to Orowan strengthening. Future work is needed to optimize laser parameters for material performance.

Acknowledgements

The authors would like to acknowledge the funding of equipment provided by the Murdock Charitable Trust (contract #2016231), Department of Energy (DOE) (DE-EE0007888-10-4) Advanced Manufacturing Office (AMO) and the Rapid Advancement in Process Intensification Deployment (RAPID) Institute. We also gratefully acknowledge the Electron Microscope Facility OSU and Advanced Technology and Manufacturing Institute (ATAMI) facility staff and director.

References

[1] Kruth J-P, Leu M-C, Nakagawa T (1998) Progress in Additive Manufacturing and Rapid Prototyping. *CIRP Annals* 47/2:525–540.
[2] Zhao C, Fezzaa K, Cunningham RW, Wen H, De Carlo F, Chen L, et al. Real-time Monitoring of Laser Powder Bed Fusion Process Using High-Speed X-ray Imaging and Diffraction. *Scientific Reports* 7/1:3602.
[3] Linebaugh K (2013) GE Brings Engine Work Back. *The Wall Street Journal* : B2–B7.
[4] Bourell D, Kruth JP, Leu M, Levy G, Rosen D, Beese AM, et al. Materials for Additive Manufacturing. *CIRP Annals* 66/2:659–681.
[5] Hirata A, Fujita T, Wen Y, Schneibel J, Liu CT, Chen M (2011) Atomic Structure of Nanoclusters in Oxide-Dispersion-Strengthened Steels. *Nature materials* 10/12:922.
[6] Zinkle SJ, Was G (2013) Materials challenges in nuclear energy. *Acta Materialia* 61/3:735–758.
[7] Kenel C, Dasargyri G, Bauer T, Colella A, Spierings AB, Leinenbach C, et al. Selective Laser Melting of an Oxide Dispersion Strengthened (ODS) γ-TiAl Alloy Towards Production of Complex Structures. *Materials and Design* 134:81–90.
[8] Odette G, Alinger M, Wirth B (2008) Recent Developments in Irradiation-Resistant Steels. *Annual Revist Material Research* 38:471–503.
[9] Hunt RM, Kramer KJ, El-Dasher B (2015) Selective Laser Sintering of MA956 Oxide Dispersion Strengthened Steel. *Journal of Nuclear Materials* 464:80–85.
[10] Ghayoor M, Lee K, He Y, Chang C-h, Paul BK, Pasebani S (2019) Selective Laser Melting of 304L Stainless Steel: role of Volumetric Energy Density on the Microstructure, Texture and Mechanical Properties. *Additive Manufacturing* :101011.
[11] Kruth J-P, Levy G, Klocke F, Childs T (2007) Consolidation Phenomena in Laser and Powder-Bed Based Layered manufacturing. *CIRP Annals* 56/2:730–759.
[12] Melnikov P, Nascimento V, Consolo L, Silva A (2013) Mechanism of Thermal Decomposition of Yttrium Nitrate Hexahydrate, Y (NO 3) 3• 6H 2 O and Modeling of Intermediate Oxynitrates. *Journal of Thermal Analysis and Calorimetry* 111/1:115–119.
[13] Ghayoor M, Lee K, He Y, Chang C-h, Paul BK, Pasebani S (2019) Microstructural Analysis of Additively Manufactured 304 L Stainless Steel Oxide Dispersion Strengthened Alloy. *Microscopy and Microanalysis* 25/S2:2594–2595.
[14] Ghayoor M, Mirzababaei S, Lee K, He Y, Chang C-h, Paul BK, et al. Strengthening of 304 L Stainless Steel by Addition of Yttrium Oxide and Grain Refinement during Selective Laser Melting. In: *30th annual international solid freeform fabrication symposium*, Austin, TX.
[15] Kou, S., 2003, Welding metallurgy, New Jersey, USA, 431–446.
[16] Guan K, Wang Z, Gao M, Li X, Zeng X (2013) Effects of Processing Parameters on Tensile Properties of Selective Laser Melted 304 Stainless Steel. *Materials & Design* 50:581–586.
[17] Wang M, Zhou Z, Sun H, Hu H, Li S (2013) Microstructural Observation and Tensile Properties of ODS-304 Austenitic Steel. *Materials Science and Engineering A* 559:287–292.
[18] ASTM. *A240/A240M-17, Standard specification for chromium and chromium-nickel stainless steel plate, sheet, and strip for pressure vessels and for general applications*, ASTM InternationalWest Conshohocken, PA.

Please cite this article as: B.K. Paul et al., Oxide dispersion strengthened 304 L stainless steel produced by ink jetting and laser powder bed fusion, CIRP Annals - Manufacturing Technology (2020), https://doi.org/10.1016/j.cirp.2020.04.071